

Article

The Influence of Aging Precipitates on the Mechanical Properties of Al–Li Alloys and Microstructural Analysis

Ganghui Li ^{1,2,3}, Wei Xiao ^{1,2,3,*}, Xiwu Li ^{1,2,3,*}, Kai Wen ^{1,2,3}, Guanjun Gao ^{1,2,3}, Lizhen Yan ^{1,2,3}, Yanan Li ^{1,2,3}, Hongwei Yan ^{1,2,3}, Yongan Zhang ^{1,2,3}, Xingquan Wang ^{1,3} and Baiqing Xiong ^{1,3}

- ¹ State Key Laboratory of Nonferrous Metals and Processes, China GRINM Group Co., Ltd., Beijing 100088, China; ghli1225@163.com (G.L.); wenkai@grinm.com (K.W.); gaoguanjun@grinm.com (G.G.); yanlizhen@grinm.com (L.Y.); liyanan@grinm.com (Y.L.); yanhongwei@grinm.com (H.Y.); zhangyongan@grinm.com (Y.Z.); wangxingquan@grinm.com (X.W.); xiongbq@grinm.com (B.X.)
- ² GRIMAT Engineering Institute Co., Ltd., Beijing 101407, China
- ³ General Research Institute for Nonferrous Metals, Beijing 100088, China
- * Correspondence: xiaowei@grinm.com (W.X.); lixiwu@grinm.com (X.L.)

Abstract: In this work, the evolution of mechanical properties of binary Al–Li alloys with four approximately equal gradient Li contents (0.91–3.98 wt.%) under aging conditions is thoroughly investigated. The alloys undergo aging treatments at 175 °C for x hours (x = 0–120 h), and the peak-aged times of the four alloys are 6 h, 12 h, 48 h and 48 h, respectively, as the Li concentration increases. Both in the solution-treated and peak-aged states, the elastic modulus of binary Al–Li alloys exhibits an approximately linear increase with increasing Li content, consistent with trends predicted by density functional theory (DFT) calculations. Due to the presence of Al₃Li precipitates, the modulus of higher-Li-concentration alloys in the peak-aged state increases by approximately 1.4–2.5% compared with that of alloys in the solution-treated state. Additionally, the study finds that increasing Li content significantly enhances the tensile strength and yield strength of the alloy but decreases its ductility, leading to a transition in fracture mode from ductile to brittle, as evidenced by a microscopic analysis of fracture surfaces. Under peak-aged (175 °C/48 h), the alloy with the highest Li content exhibits the maximum tensile strength of 341 MPa and a yield strength of 296 MPa, while its elongation is the lowest at 2.1%. These findings contribute to a deeper understanding of the effects of aging precipitates on the mechanical properties of Al–Li alloys, providing fundamental guidance for the design of future generations of Al–Li alloys.

Keywords: binary Al–Li alloy; elastic modulus; mechanical properties; microstructure analysis



Citation: Li, G.; Xiao, W.; Li, X.; Wen, K.; Gao, G.; Yan, L.; Li, Y.; Yan, H.; Zhang, Y.; Wang, X.; et al. The Influence of Aging Precipitates on the Mechanical Properties of Al–Li Alloys and Microstructural Analysis. *Metals* **2024**, *14*, 506. <https://doi.org/10.3390/met14050506>

Academic Editors: Andrii Kostryzhev and Roberto Figueiredo

Received: 12 March 2024

Revised: 22 April 2024

Accepted: 24 April 2024

Published: 26 April 2024



Copyright: © 2024 by the authors. Licensee MDPI, Basel, Switzerland. This article is an open access article distributed under the terms and conditions of the Creative Commons Attribution (CC BY) license (<https://creativecommons.org/licenses/by/4.0/>).

1. Introduction

Aluminum–lithium alloys are widely used in aerospace applications due to their low density, high specific strength, excellent resistance to fatigue crack extension and stress corrosion resistance [1–4]. Among them, Li, as the lightest metal element in nature, can effectively reduce the density of the alloy. Studies have shown that every 1 wt.% of Li added to aluminum can reduce the density of the alloy by 3% and increase the modulus of elasticity by 6% [5,6], which is a significant advantage in the lightweighting of the alloy compared with conventional aluminum alloys.

Al–Li alloy is an aging-strengthened alloy, and its aging precipitation behavior is affected by key factors such as the content of Li elements [7] and aging conditions [8,9]. Early on, Noble [10] investigated elastic modulus variation in alloys with different Li contents, revealing that an increase in Li concentration enhances the elastic modulus of the alloy. However, previous studies lacked detailed mechanistic analyses and corresponding investigations into mechanical properties such as tensile strength. Xue et al. [11] investigated the mechanism of enhancing the elastic modulus of an alloy at a single concentration, and

found that Young's modulus of a binary Al–Li alloy is dependent on both the Li concentration and the heat treatment conditions. Gao et al. [12] pointed out that the increase in the elastic modulus of an Al–Li alloy in the aging stage is due to the precipitation of δ' -Al₃Li with strong covalent bonds. Starke [13] and Jeon et al. [14] highlighted that Li existed in the form of a solid solution or aging precipitated phase, Al₃Li, which could increase the elastic modulus of the alloy. Based on the research mentioned above, many research groups have tried to regulate the properties of alloys by further altering the alloying elements and heat treatment processes [3,15,16]. Hirosawa et al. [17] suggested that, by adding Mg element to Al–Li alloy to reduce the solid solubility of Li in the matrix, the solid solution's strengthening of the alloy can be improved, and the coherent strengthening phase δ' precipitates in the early aging of the aluminum alloy. The concentration of the main alloying element affects the age-hardening ability of the alloy, leading first to a decrease and then a significant increase in age-hardening ability as the Cu/Li ratio is increased [18]. Deschamps [19] and Katsikis [20] found that in alloys with higher Li content, the precipitation of the δ' phase results in higher strength of the alloy. Chai et al. [21] pointed out that the precipitation of the δ' phase in binary Al–Li alloys is closely related to the increase in Li content in the Li-rich region. Xie et al. [22] highlighted that when the Li content is high, the δ' phase will coarsen with increasing aging temperatures, ultimately leading to a significant reduction in material strength. Al–Li alloys [23] with low Li content exhibit excellent specific strength in the T83 states. Also, some research [24,25] shows that Al–Li alloys exhibit optimal mechanical properties at 170–175 °C. However, when the aging temperature exceeds 175 °C, the hardness sharply decreases. Therefore, the aging temperature of 175 °C is often applied in the study of Al–Li alloys.

Up to now, previous research has clearly indicated the significant role of Li content and precipitates in enhancing the properties of Al–Li alloys. However, there is still insufficient understanding of the effects of different Li contents and aging conditions on the mechanical properties of the alloy. For instance, the differences in the influence of solid solution and aging states on the alloy modulus, as well as the impact of Li content on other mechanical properties such as tensile strength, yield strength, and fracture morphology, lack systematic investigation. In this study, we will meticulously design four alloy compositions with varying Li concentrations suitable for experimental preparation and computational simulation, to comprehensively investigate the impact of Li content on the mechanical properties of the alloy, beyond the scope of modulus properties alone. The extent of differences in moduli due to solid solution and aging states will be revealed and further validated through density functional theory (DFT) theoretical calculations. Discrepancies in tensile performance and their corresponding microstructural characterization will also be elucidated. This will offer a more comprehensive understanding, serving as fundamental guidance for future Al–Li alloy design.

2. Methods

2.1. Experimental Methods

Binary Al–Li alloy ingots with Li contents of 0.85 wt.%, 1.70 wt.%, 2.55 wt.% and 3.40 wt.% were prepared via the fusion casting method, and they had dimensions of $\varnothing 13.3 \text{ mm} \times 300 \text{ mm}$. The concentrations of the Al–Li alloys used in the experiments were chosen based on a theoretical calculation model that will be described later, ensuring consistency between the experimental and theoretical alloy concentrations. Different homogenization regimes were determined based on the test results of differential scanning calorimetry (DSC) and phase diagrams of binary Al–Li alloys. After the ingots were homogenized, the ingots were extruded into slatted specimens with a cross-section size of $15 \text{ mm} \times 60 \text{ mm}$ during the extrusion process. Subsequently, binary Al–Li alloys with varying compositions underwent solid-solution treatment under different parameters, followed by immediate quenching in cold water. The solid-solution treatment was then succeeded by aging at 175 °C for a duration of 0–120 h. The elastic modulus of the alloy was measured using the RFDAHT1050 elastic modulus, the resonance frequency

and a damping analyzer. The specimen dimensions for the elastic modulus test were 75 mm × 25 mm × 5 mm. The alloy density was determined using the drainage method. Tensile properties were evaluated using a CMT4303 microcomputer-controlled universal tensile testing machine (MTS, Shenzhen, China) with a tensile speed of 2 mm/min. The tensile specimen size was M10-ø5 mm. Three parallel samples for each alloy were used in the modulus of elasticity and tensile properties tests. The microstructure was observed via scanning electron microscopy (SEM, JEOL JSM 7001F, Tokyo, Japan, 15 kV) and transmission electron microscopy (TEM). The chemical compositions were determined using an electron probe micro-analyzer (EPMA). The actual compositions of the alloys used are shown in Table 1, demonstrating high consistency with the chosen elemental contents.

Table 1. Nominal elemental contents of the Al–Li alloys.

Alloy No.	Nominal Elemental-Content (wt.%)	
	Li	Al
1#	0.91	Bal.
2#	1.59	Bal.
3#	2.44	Bal.
4#	3.98	Bal.

2.2. Computational Methods

First-principles calculations based on DFT were performed using the Vienna *Ab-initio simulation* package (VASP 6.1.0) computational software [26,27]. Electron exchange and correlation were treated within the framework of generalized gradient approximation (GGA) in the Perdew–Burke–Ernzerhof (PBE) form [28]. Supercell (2 × 2 × 2) structures with different Li contents were constructed using the special quasi-random structures (SQS) [29,30] method to match the experimental Li concentrations. The Li solid solution concentrations were 3.13 at.%, 6.25 at.%, 9.38 at.% and 12.50 at.% in the modeling, which were consistent with the experimental concentrations. To ensure high accuracy, a large cutoff of 500 eV and a sufficient number of *k*-points were employed for all the computational tasks. During the atomic relaxation process, the convergence standards of the total energy and force were less than 1.0×10^{-5} eV and 1.0×10^{-2} eV/Å, respectively.

3. Results and Discussion

3.1. Aging Hardening Curves for Binary Al–Li Alloys

In accordance with the DSC test results, the homogenization regimes were investigated for alloys with different compositions. Because of the low Li content, there was no second phase in the ingots of 1# and 2# alloys, so homogenization was not required. According to the DSC test of 3# and 4# alloys, the final homogenization regimes was determined as shown in Table 2.

Table 2. Optimized homogenization regimes of the binary Al–Li alloys.

Alloy No.	Homogenization Regimes
1#	-
2#	-
3#	525 °C/24 h
4#	525 °C/24 h

To verify the influence of precipitation on the mechanical properties of the alloy, the aging hardening curve of the alloy was firstly explored. The hardening curve of the binary Al–Li alloy after 175 °C/120 h aging treatment after solid-solution treatment is shown in Figure 1. The hardness values are in descending order: 4#, 3#, 2# and 1#. It is well known that δ' (Al₃Li), as one of the main strengthening phases in Al–Li alloys, can disperse and precipitate during the aging process, resulting in the strengthening and

hardening of the alloy [31]. As shown in Figure 1, the hardness of alloy 1# did not exhibit significant improvement after aging treatment, indicating the limited effectiveness of aging strengthening. This could be attributed to the low Li content in alloy 1# and the scarcity of precipitated second-phase particles, resulting in a negligible impact on aging strengthening. The hardness of alloy 2# increased initially during aging, reaching its peak after 12 h, and then stabilized, with a hardness value stabilizing at around 62 MPa. The increase in hardness of the alloy after aging is primarily attributed to the obtention of a supersaturated solid solution after solid solution treatment, followed by the uniform precipitation of the second phase during aging treatment, resulting in an aging strengthening effect and a hardness increase. The hardness of alloy 3# rapidly increases with increasing aging time, maintaining a hardness value of about 110 HV after 48 h of aging, which is higher than that of alloy 2# after aging. Hence, it can be inferred that an increase in Li content contributes to an enhancement in the hardness of the alloy. The microhardness of alloy 4# further increased with aging time. After aging at 175 °C for 48 h, the microhardness of the alloy increased from 60 HV to 141 HV, reaching its peak. For alloys 3# and 4# with higher Li content, the hardness remained stable in the late aging stage, mainly due to the gradual transformation of the unstable δ' phase to the stable δ (AlLi) phase [32], indicating a minimal impact on hardness. Through a comparison of the aging hardening curves of different alloys, it can be concluded that increasing Li content significantly enhances the microhardness of the alloy.

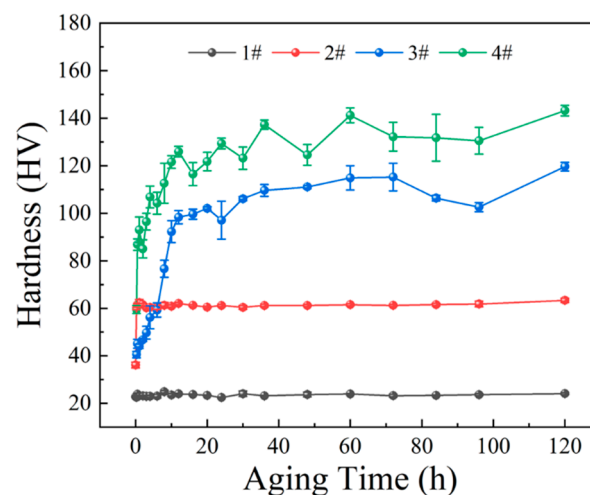


Figure 1. Age hardening curves of binary Al-Li alloys at 175 °C.

3.2. Determination of Density and Modulus of Binary Al-Li Alloys

Figure 2 presents the density measurements of the cast alloys with varying Li contents (0~3.4 wt.%). The alloy density demonstrates a linear relationship with Li concentration, with a decrease of 3% in density for every 1% increase in Li content, consistent with other experimental findings [33]. The elastic moduli and specific moduli of the solid solution- and age-treated alloys are presented in Figure 3, where the specific moduli shown were calculated by dividing the moduli by the measured density. Previous investigations have demonstrated that the quenching process of high-concentration alloys results in a minor formation of the δ' phase, which does not significantly impact subsequent modulus measurements [32]. The results of the elastic modulus measurement of the solid-solution state are shown in Figure 3a. It can be seen that as the Li concentration increases from 0.85 wt.% to 3.4 wt.%, the elastic modulus of the alloy increases from 72.8 GPa to 80.3 GPa, and the specific modulus increases from 27.5 GPa/g·cm⁻³ to 33.7 GPa/g·cm⁻³. The elastic modulus of aluminum alloy in the solid-solution state is mainly determined by the interaction between solute and matrix atoms. When the second phase precipitates during aging, the elastic modulus is affected by the size and volume fraction of the second phase.

For the peak-aged state, there was no significant change in modulus values for alloys with a Li content below 1.7 wt.%, as shown in Figure 3b. However, due to the presence of precipitated phases, the modulus of higher-Li-concentration alloys in the peak-aged state was about 1.4% to 2.5% higher than that of alloys in the solid-solution state, indicating that aging heat treatment could further enhance an alloy's elastic modulus. In a previous study, Xue et al. [11] noted that the elastic modulus of binary Al–Li alloys with 4.2% Li content increased during the transition from the solid-solution to the aging state. This might be related to the Li-rich clusters precipitated by aging. Overall, with the increase in Li concentration, the elastic modulus of the peak-aged alloy increased from 71.8 GPa to 82.6 GPa, and the specific modulus increased from 27.1 GPa/g·cm⁻³ to 34.7 GPa/g·cm⁻³. This indicates that the addition of the Li element can increase the elastic modulus and specific modulus of aluminum alloy.

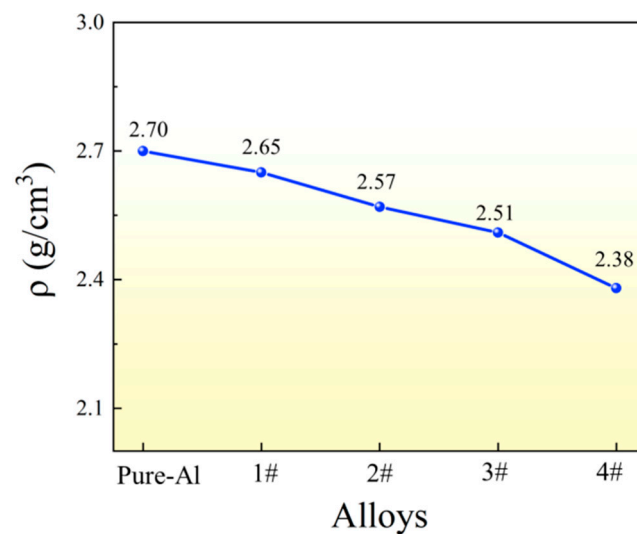


Figure 2. Density curve of binary Al–Li alloys.

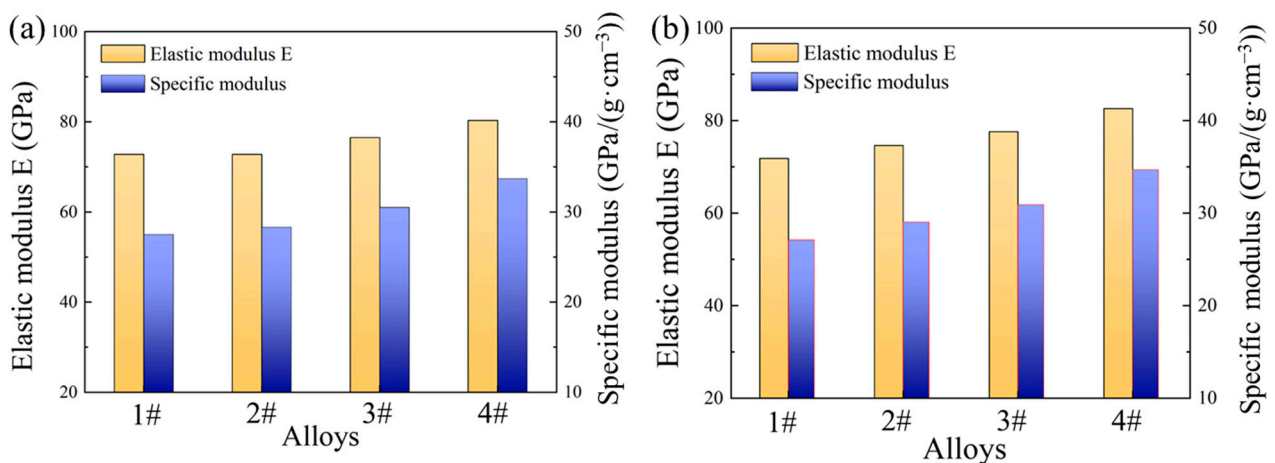


Figure 3. Elastic moduli and specific moduli of binary Al–Li alloys: (a) solid solution; (b) peak-aged state.

In Figure 4, we compare the experimentally obtained elastic modulus, E , of binary Al–Li alloys in different heat treatment states with the elastic modulus calculated using DFT for a disordered solid solution model. The DFT theory predicted that the elastic modulus of the binary Al–Li solid solution gradually increased from 80.2 GPa to 88.4 GPa with increasing Li content. Although the ideal crystal model used in the calculation often yields a higher elastic modulus compared with the experimental values [34], it still shows a trend

consistent with the results of the experiment. Furthermore, fitting curves were generated for the elastic modulus, E , corresponding to the theoretical calculations and experimental solid-solution and peak-aged states depicted in Figure 4, yielding slopes of 0.9, 1.1, and 0.8. The above research findings indicate that the modulus of the alloy in the peak-aged state increases most rapidly and has the largest slope. Under peak-aged conditions, the alloy's elastic modulus reaches 88.4 GPa, representing an increase of 5.8 GPa compared with that in the modulus of the solid-solution alloy. Additionally, DFT calculations revealed an elastic modulus of 110.2 GPa for aging-precipitated phase δ' , which is significantly greater than that of the binary Al–Li alloy at maximum solid solubility, further confirming that the δ' phase effectively enhances the elastic modulus of Al–Li alloys [35]. Therefore, by controlling both matrix composition and the heat treatment process, it is possible to improve an alloy's elastic modulus.

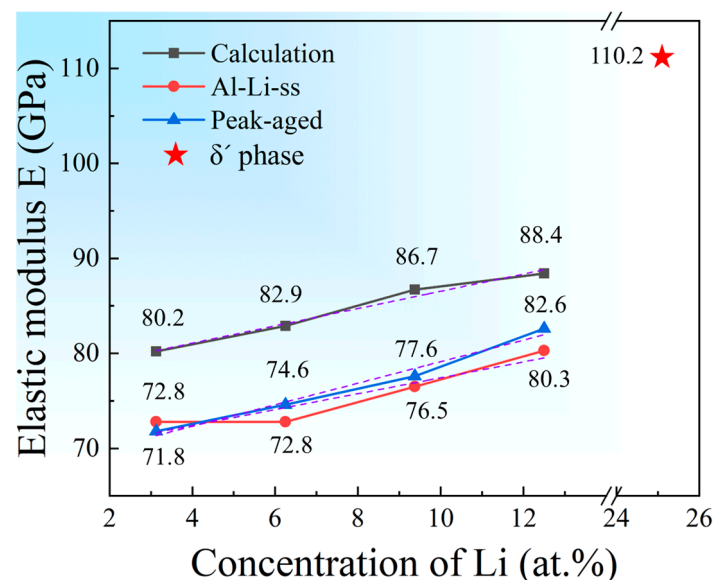


Figure 4. Comparison of the elastic modulus, E , in theoretical calculations with experimental solid-solution and peak-aged states for binary Al–Li alloys. The calculated elastic modulus, E , of δ' is also included. The purple dashed line represents the curve fitting of the elastic modulus.

3.3. Tensile Properties of Binary Al–Li Alloys

In the process of alloy research, tensile properties are also considered. Figure 5 shows the tensile properties of the alloy in the peak-aged state. Under peak-aged conditions, the tensile strength, yield strength, and elongation of alloy 1# were 65 MPa, 45 MPa, and 36.4%, respectively. When the Li content increases to 1.59%, the tensile strength and yield strength of alloy 2# were 93.5 MPa and 54.5 MPa, and the elongation decreases to 25.5%. With the increase in Li content, the tensile strength, yield strength, and elongation of alloy 3# were 274 MPa, 233 MPa and 3.0%, respectively. At this point, there was a significant decrease in elongation, indicating brittle fracture. Upon further increasing the Li content to 3.98 wt.%, the tensile strength and yield strength of alloy 4# increased to 341 MPa and 296 MPa, respectively, while the elongation decreases to 2.1%. This suggests that alloy 4# sacrificed its ductility while increasing its strength. It can be concluded that as the Li content increases, the alloy's tensile strength and yield strength exhibit a significant increase, while there is a notable decrease in elongation, as depicted in Figure 5. This observation aligns with the findings of previous studies [36], which indicate that the δ' phase, serving as the primary strengthening phase in Al–Li alloys, also acts as a brittle phase. Consequently, while enhancing the alloy's strength, the precipitation of this phase concurrently increases its brittleness.

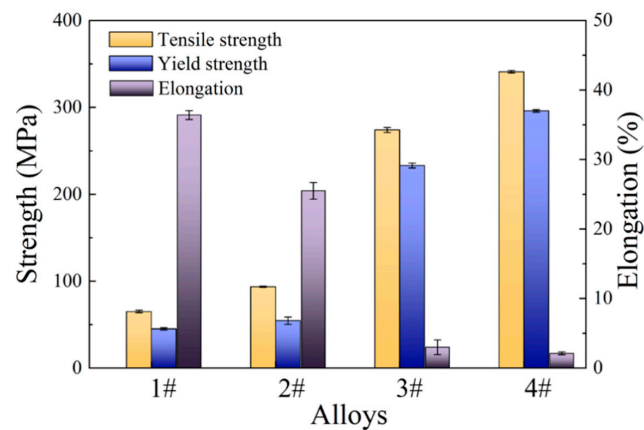


Figure 5. Tensile properties of peak-aged binary Al-Li alloys.

3.4. Fracture Surface Observation of Peak-Aged Alloys

In order to analyze the fracture mode, SEM observation was conducted on the fracture of the alloy under the peak-aged state, as depicted in Figure 6. Alloy 1# exhibited a pronounced neck contraction phenomenon during peak aging, and its fracture displayed an abundance of ductile grooves with the minimal presence of tear edges, indicative of a micropore polymerization mechanism and characteristic of ductile fracture. The fracture of alloy 2# contained a large number of small and shallow dimples, and most grains were cut off. Therefore, according to the propagation path of the crack, the type of fracture of alloy 2# was trans-granular fracture, so it also underwent ductile fracture. The neck contraction phenomenon also occurred before the fracture of alloy 2#, but compared with 1# alloy, the plastic deformation was weaker, so the brittleness of the alloy increased. With the increase in plastic deformation, the dimples began to grow and polymerize with adjacent dimples, then gradually spread into microcracks, which eventually led to the fracture of the tensile samples. A similar experimental phenomenon was also reported by Huang et al. [37]. There were no obvious plastic deformation traces in the macro fracture of alloy 3#. The fracture morphology of alloy 3# presented a polyhedral rock-like pattern, with distinct grains and strong three-dimensional sense. Therefore, 3# alloy belongs to intergranular fracture in brittle fracture, and the plasticity is significantly lower than that of alloy 2#. The fracture morphology of alloy 4# is partly rock sugar-like, with intergranular fracture. Therefore, alloy 4# exhibited increased brittleness. The findings suggest that as the Li element content increases, the toughness of the Al-Li alloy decreases.

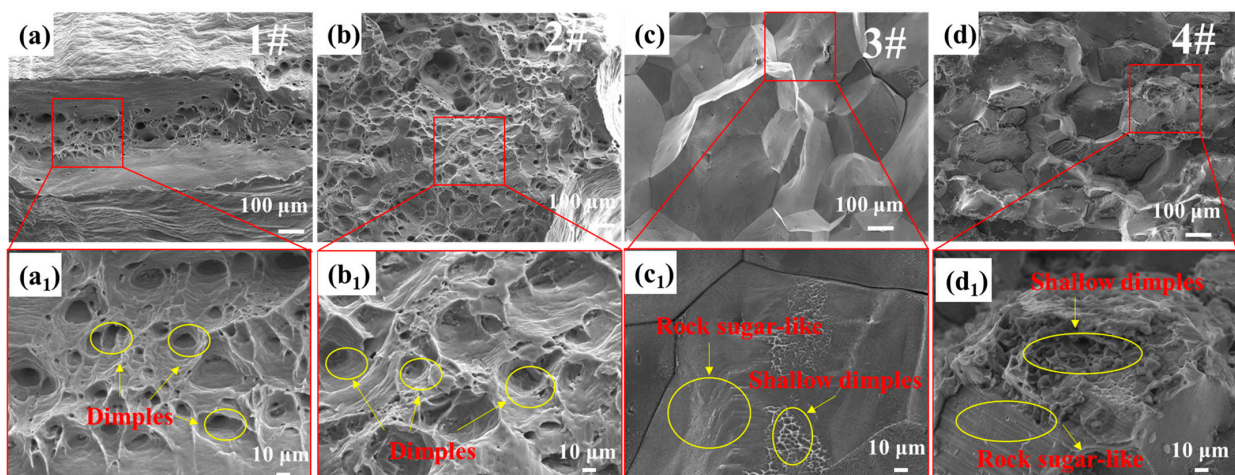


Figure 6. Tensile fracture morphology of peak-aged alloys: (a–d) low-magnification images of different alloys; (a₁–d₁) corresponding high-magnification images.

3.5. Microstructure Analysis of Peak-Aged Alloys

As the main strengthening phase in binary Al–Li alloys, the presence of the δ' phase endows the alloy with superior mechanical properties [38]. To further investigate the effect of precipitated phases on the mechanical properties of the alloy, transmission electron microscopy (TEM) observations were conducted on four alloys in peak-aged condition. Figure 7 shows the TEM micrographs and corresponding selected area electron diffraction (SAED) patterns of alloys 1# and 2# in the peak-aged condition (175 °C/6 h and 175 °C/12 h). Based on the electron microscopy results in Figure 7a–c, it can be observed that no δ' phase precipitation was found in alloy 1#. Combined with the elastic modulus results in Figure 3, it can be concluded that the elastic modulus of alloy 1# in the peak-aged state was similar to or even lower than that in the solid-solution state, indicating that aging did not lead to an increase in modulus of alloy 1#. It is currently speculated that this may have been due to the low Li content, leading to the alloy being primarily strengthened via solid solution strengthening. As for alloy 2#, the Al_3Li precipitation phase can be observed in the dark-field image, SAED pattern (Figure 7e), and high-resolution transmission electron microscope (HRTEM) image (Figure 7f). Figure 7e shows the dark-field image of the δ' (Al_3Li) phase with a higher density of the fine δ' phase being uniformly distributed in the matrix of alloy 2#. In this alloy, the size of the δ' phase was less than 10 nm. Diffraction spots of the δ' phase were observed along the $[100]_{\text{Al}}$ direction in alloy 2#, indicating that these fine δ' precipitates strengthened the alloy through the aging hardening mechanism [39], thereby improving the elastic modulus and mechanical properties of the alloy. In the HRTEM image of alloy 2# (Figure 7f), the presence of the δ' phase can also be clearly observed. It is further demonstrated that the enhancement in the elastic modulus and mechanical properties was correlated with the precipitation of the δ' phase.

Figure 8 shows the TEM images of alloys the 3# and 4# under peak-aging and the corresponding average size statistics of Al_3Li precipitated phases. According to the quantitative analysis results of alloys 3# and 4# with high Li content, the increase in Li content can promote the growth of the δ' phase, which can improve the strength of the alloy while reducing the toughness. δ' phases can be clearly observed in the bright-field images (Figure 8a₁,b₁) and dark-field images (Figure 8a₂,b₂) of alloys 3# and 4#. Diffraction spots of the δ' phase can be noted along the $[100]_{\text{Al}}$ incident direction for both 3# (Figure 8a₂) and 4# (Figure 8b₂) alloys. The TEM observation revealed a uniform distribution of the spherical δ' phase within the matrix [40]. As depicted in Figure 8a₄, the average size of the δ' phase at peak aging was measured to be 19.7 nm in alloy 3#, which is larger than that in alloy 2#. Consequently, compared with alloy 2#, alloy 3# exhibited a higher elastic modulus and more tensile properties. However, due to the increase in both size and the number of brittle δ' phases, the brittleness of alloy 3# also increased. As shown in Figure 8b₄, with the further increase in Li content up to a concentration of approximately 3.98 wt.%, more precipitated δ' phases were observed during peak aging for alloy 4# along with some presence of the δ phase as well. The average size of the δ' phases at peak aging for alloy #4 measured approximately 24.9 nm, indicating a further increase compared with that observed in alloy 3#. Under peak-aged conditions, the size of the δ' phase in binary Al–Li alloys gradually increases with the increase in Li content. Consequently, this leads to an enhanced elastic modulus and enhanced tensile properties; however, it also results in an elevated level of brittleness. This further emphasizes that plasticity behavior primarily depends on precipitation characteristics exhibited by precipitated phases during peak aging [41].

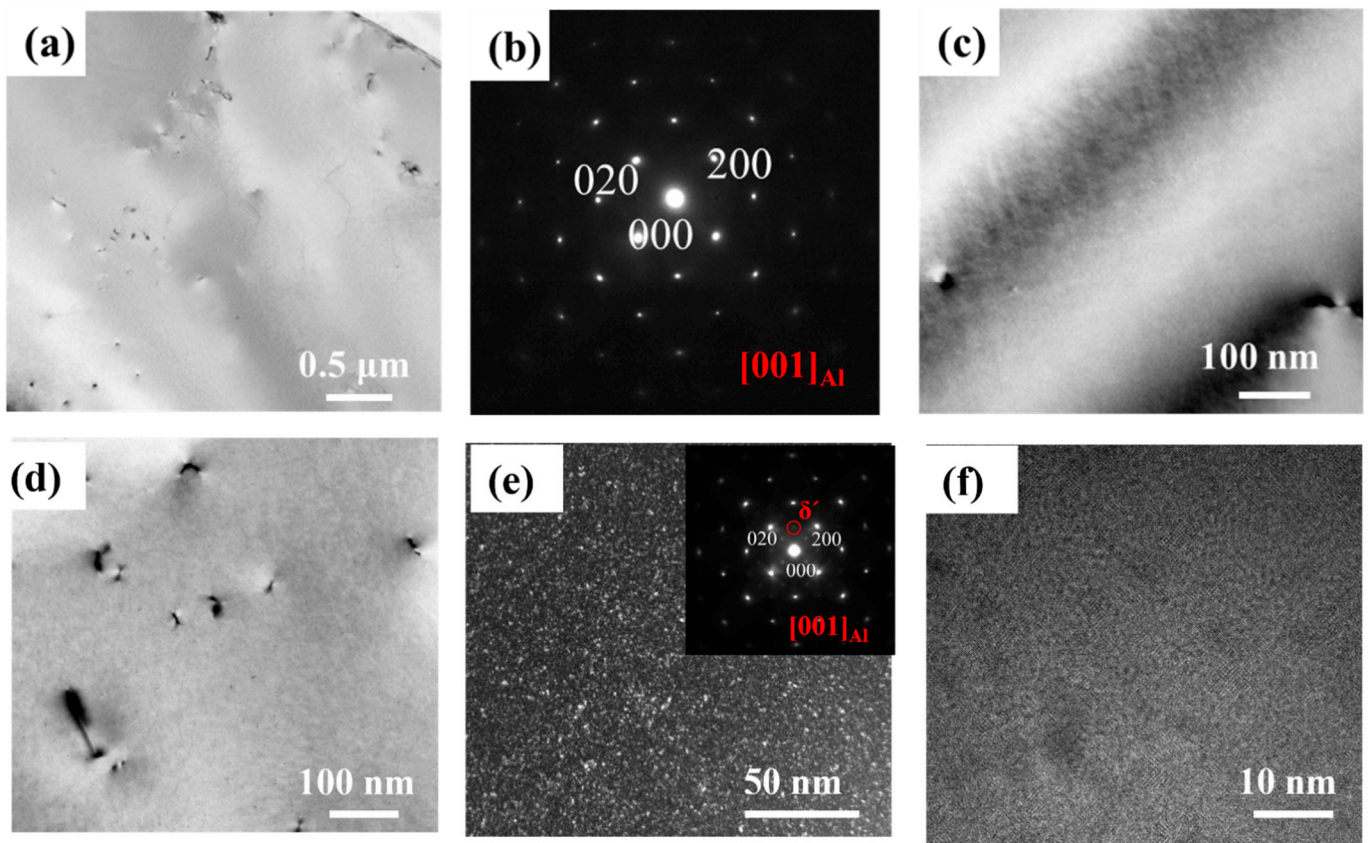


Figure 7. TEM images of peak-aged alloys: (a,c) Bright-field images and (b) corresponding SAED patterns $[001]_{Al}$ of 1# alloys; (d) bright-field image, (e) dark-field image with SAED patterns, and (f) HRTEM of 2# alloys.

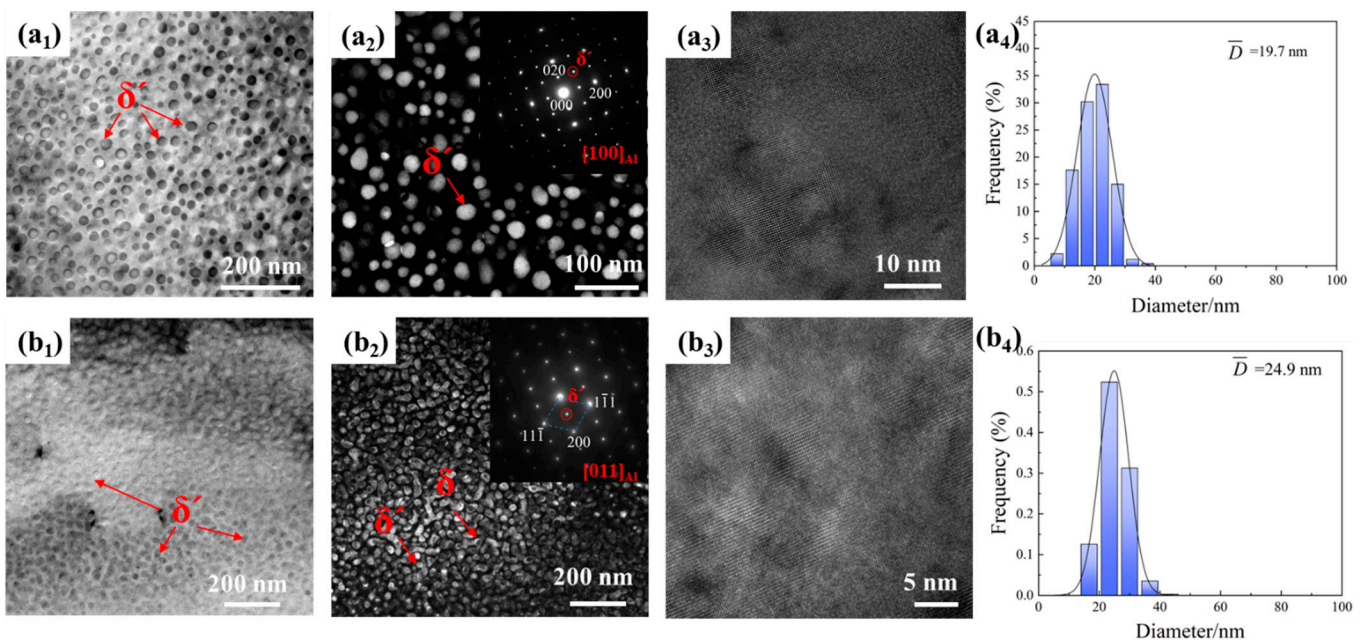


Figure 8. TEM images of (a₁–a₃) and (b₁–b₃) alloys 4#: (a₁,b₁) δ' phases in bright-field images; (a₂,b₂) δ' phases in dark-field images; (a₃,b₃) HRTEM images. (a₄,b₄) represent the size distribution of the δ' phase for alloys 3# and 4#, respectively.

4. Conclusions

In this study, the influence of aging precipitates on the mechanical properties of binary Al–Li alloys with four approximately equal gradient Li contents (0.91–3.98 wt.%) was thoroughly investigated. The alloys were subjected to solution treatment followed by aging at 175 °C for 120 h. The effects were analyzed through measurements of the elastic modulus, tensile testing, fracture surface analysis, and microstructural observation, yielding the following results:

- (1) Both in the solution-treated and peak-aged states, the elastic modulus of binary Al–Li alloys showed an approximately linear increase with increasing Li content, consistent with trends predicted via DFT calculations. Under peak-aged conditions, the elastic modulus of the alloys increased from 71.8 GPa for alloy 1# to 82.6 GPa for alloy 4#. Due to the presence of precipitates, the modulus of higher—Li-concentration alloys in the peak-aged state increased by approximately 1.4–2.5% compared with that of alloys in the solution-treated state.
- (2) Increasing Li content significantly enhances the tensile strength and yield strength of an alloy but decreases its ductility, leading to a transition in the fracture mode from ductile to brittle, as evidenced by the microscopic analysis of fracture surfaces. Under peak-aged conditions (175 °C/48 h), alloy 4#, with the highest Li content, exhibited the maximum tensile strength of 341 MPa and a yield strength of 296 MPa, while its elongation was the lowest at 2.1%.
- (3) No δ' phase was observed in alloy 1# during peak aging, indicating mainly solid solution strengthening. However, alloys 2#, 3#, and 4# all exhibited the presence of the δ' phase as observed through TEM, accompanied by an increase in the elastic modulus, suggesting that these three alloys were primarily strengthened by precipitation hardening. Alloys 3# and 4# exhibited significant age-hardening and strengthening effects, with hardness increasing notably with aging time and stabilizing in later stages. At peak aging (175 °C/48 h), the hardness of alloy 3# stabilized at approximately 110 HV, while alloy 4# reached a hardness of around 141 HV.

This comprehensive analysis contributes to a deeper understanding of the effects of aging precipitates on the mechanical properties of Al–Li alloys, providing valuable insights for further research and development in this field.

Author Contributions: Conceptualization, G.L. and W.X.; Data curation, X.L. and K.W.; Formal analysis, G.L.; Funding acquisition, W.X. and X.L.; Investigation, G.L., L.Y., Y.L. and H.Y.; Methodology, G.L.; Resources, W.X. and G.G.; Software, G.L.; Supervision, W.X., X.L., K.W., G.G., H.Y., Y.Z., X.W. and B.X.; Validation, X.W. and B.X.; Visualization, L.Y., Y.L. and Y.Z.; Writing—original draft, G.L.; Writing—review and editing, W.X. All authors have read and agreed to the published version of the manuscript.

Funding: This work was financially supported by the National Key R&D Program of China (No. 2020YFF0218200).

Data Availability Statement: The data presented in this study are available on request from the corresponding author. The data are not publicly available due to privacy.

Acknowledgments: The Innovation Fund Project of GRINM and other related projects.

Conflicts of Interest: All authors were employed by the company China GRINM Group Co., Ltd. Authors Ganghui Li, Wei Xiao, Xiwu Li, Kai Wen, Guanjun Gao, Lizhen Yan, Yanan Li, Hongwei Yan and Yongan Zhang were employed by the company GRIMAT Engineering Institute Co., Ltd. All authors were employed by the company General Research Institute for Nonferrous Metals. All authors declare that the research was conducted in the absence of any commercial or financial relationships that could be construed as a potential conflict of interest.

References

1. Yang, X.; Wang, M.; Zhang, C.; Xue, C.; Guo, Y.; Liu, X. Achieving high strength and ductility of Al-Cu-Li alloy via creep aging treatment with different pre-strain levels. *Mater. Today Commun.* **2021**, *29*, 102898–102910. [[CrossRef](#)]
2. Wang, S.; Zhang, C.; Li, X.; Wang, J. Heterophase interface dominated deformation and mechanical properties in Al-Cu-Li Alloys. *Adv. Theory Simul.* **2021**, *4*, 2100059–2100070. [[CrossRef](#)]
3. Ma, J.; Liu, X.; Yan, D.; Rong, L. A novel GP-Li precursor and the correlated precipitation behaviors in Al-Cu-Li alloys with different Cu/Li Ratio. *Acta Mater.* **2023**, *243*, 118442–118458. [[CrossRef](#)]
4. Xue, C.; Zhang, Y.; Mao, P.; Liu, C.; Guo, Y.; Qian, F.; Zhang, C.; Liu, K.; Zhang, M.; Tang, S.; et al. Improving Mechanical Properties of Wire Arc Additively Manufactured AA2196 Al-Li Alloy by Controlling Solidification Defects. *Addit. Manuf.* **2021**, *43*, 102019. [[CrossRef](#)]
5. Rioja, R.J.; Liu, J. The Evolution of Al-Li Base Products for Aerospace and Space Applications. *Metall. Mater. Trans. A* **2012**, *43*, 3325–3337. [[CrossRef](#)]
6. Elagin, V.I.; Zakharov, V.V. Modern Al-Li Alloys and Prospects of Their Development. *Met. Sci. Heat Treat.* **2013**, *55*, 184–190. [[CrossRef](#)]
7. Decreus, B.; Deschamps, A.; De Geuser, F.; Donnadieu, P.; Sigli, C.; Weyland, M. The Influence of Cu/Li Ratio on Precipitation in Al-Cu-Li-x Alloys. *Acta Mater.* **2013**, *61*, 2207–2218. [[CrossRef](#)]
8. Duan, S.; Guo, F.; Wu, D.; Wang, T.; Tsuchiya, T.; Matsuda, K.; Zou, Y. Influences of Pre-Rolling Deformation on Aging Precipitates and Mechanical Properties for a Novel Al-Cu-Li Alloy. *J. Mater. Res. Technol.* **2021**, *15*, 2379–2392. [[CrossRef](#)]
9. Rodgers, B.I.; Prangnell, P.B. Quantification of the Influence of Increased Pre-Stretching on Microstructure-Strength Relationships in the Al-Cu-Li Alloy AA2195. *Acta Mater.* **2016**, *108*, 55–67. [[CrossRef](#)]
10. Noble, B.; Harris, S.J.; Dinsdale, K. The elastic modulus of aluminum-lithium alloys. *J. Mater. Sci.* **1982**, *17*, 461–468. [[CrossRef](#)]
11. Xue, C.; Zhang, Y.; Wang, S.; Tian, G.; Yang, X.; Ke, Y.; Xie, Z.; Wang, J. Achieving Highest Young's Modulus in Al-Li by Tracing the Size and Bonding Evolution of Li-Rich Precipitates. *J. Mater. Sci. Technol.* **2023**, *145*, 125–135. [[CrossRef](#)]
12. Gao, Y.J.; Mo, Q.F.; Chen, H.N.; Huang, C.G.; Zhang, L.N. Atomic Bonding and Mechanical Properties of Al-Li-Zr Alloy. *Mater. Sci. Eng. A* **2009**, *499*, 299–303. [[CrossRef](#)]
13. Starke, E.A.; Sanders, T.H. New Approaches to Alloy Development in the Al-Li System. *J. Met.* **1981**, *33*, 24–33.
14. Jeon, S.M.; Kim, J.D.; Park, J.K.; Lee, S.S. Quantitative Analysis of Elastic Property of Al-Li Alloys Using Ultrasonic Velocity Measurement and Tem. In *Review of Progress in Quantitative Nondestructive Evaluation*; Springer: Berlin/Heidelberg, Germany, 1993.
15. Zhang, X.; Zhang, L.; Wu, G.; Liu, W.; Shi, C.; Tao, J.; Sun, J. Microstructural Evolution and Mechanical Properties of Cast Al-2Li-2Cu-0.5Mg-0.2Zr Alloy during Heat Treatment. *Mater. Charact.* **2017**, *132*, 312–319. [[CrossRef](#)]
16. Zhang, X.; Wang, H.; Yan, B.; Zou, C.; Wei, Z. The Effect of Grain Refinement and Precipitation Strengthening Induced by Sc or Er Alloying on the Mechanical Properties of Cast Al-Li-Cu-Mg Alloys at Elevated Temperatures. *Mater. Sci. Eng. A* **2021**, *822*, 141641. [[CrossRef](#)]
17. Hirosawa, S.; Sato, T.; Kamio, A. Effects of Mg Addition on the Kinetics of Low-Temperature Precipitation in Al-Li-Cu-Ag-Zr Alloys. *Mater. Sci. Eng. A* **1998**, *242*, 195–201. [[CrossRef](#)]
18. Joh, C.-H.; Yamada, K.; Miura, Y. Effect of Sc-Addition on the Coarsening Behavior of Al₃Li Precipitates in Al-Li Alloys. *Mater. Trans. JIM* **1999**, *40*, 439–442. [[CrossRef](#)]
19. Deschamps, A.; Garcia, M.; Chevy, J.; Davo, B.; De Geuser, F. Influence of Mg and Li Content on the Microstructure Evolution of Al-Cu-Li Alloys during Long-Term Ageing. *Acta Mater.* **2017**, *122*, 32–46. [[CrossRef](#)]
20. Katsikis, S.; Noble, B.; Harris, S.J. Microstructural Stability during Low Temperature Exposure of Alloys within the Al-Li-Cu-Mg System. *Mater. Sci. Eng. A* **2008**, *485*, 613–620. [[CrossRef](#)]
21. Chai, Z.; Meng, C. Small-Angle X-ray Scattering Study of the Interfacial Characteristics Between δ' Phase and Matrix in Al-2.70 mass% Li Alloy. *J. Appl. Crystallogr.* **1998**, *31*, 7–9. [[CrossRef](#)]
22. Xie, B.; Huang, L.; Xu, J.; Su, H.; Zhang, H.; Xu, Y.; Li, J.; Wang, Y. Effect of the Aging Process and Pre-Deformation on the Precipitated Phase and Mechanical Properties of 2195 Al-Li Alloy. *Mater. Sci. Eng. A* **2022**, *832*, 142394. [[CrossRef](#)]
23. Balducci, E.; Ceschini, L.; Messieri, S.; Wenner, S.; Holmestad, R. Effects of Overaging on Microstructure and Tensile Properties of the 2055 Al-Cu-Li-Ag Alloy. *Mater. Sci. Eng. A* **2017**, *707*, 221–231. [[CrossRef](#)]
24. Yan, S.; Wang, R.; Peng, C.; Cai, Z.; Peng, X.; Lv, P.; Li, X. Microstructural evolution and mechanical properties of the rapidly-solidified and hot-extruded 2196 Al-Li alloy. *J. Alloys Compd.* **2024**, *988*, 174285. [[CrossRef](#)]
25. Li, H.; Li, X.; Li, Y.; Xiao, W.; Wen, K.; Li, Z.; Zhang, Y.; Xiong, B. Machine learning assisted design of aluminum-lithium alloy with high specific modulus and specific strength. *Mater. Des.* **2023**, *225*, 111483. [[CrossRef](#)]
26. Kresse, G.; Joubert, D. From Ultrasoft Pseudopotentials to the Projector Augmented-Wave Method. *Phys. Rev. B* **1999**, *59*, 1758–1775. [[CrossRef](#)]
27. Kresse, G.; Furthmüller, J. Efficiency of Ab-Initio Total Energy Calculations for Metals and Semiconductors Using a Plane-Wave Basis Set. *Comput. Mater. Sci.* **1996**, *6*, 15–50. [[CrossRef](#)]
28. Perdew, J.P.; Burke, K.; Ernzerhof, M. Generalized Gradient Approximation Made Simple. *Phys. Rev. Lett.* **1996**, *77*, 3865–3868. [[CrossRef](#)]
29. Zunger, A.; Wei, S.-H.; Ferreira, L.G.; Bernard, J.E. Special quasirandom structures. *Phys. Rev. Lett.* **1990**, *65*, 4. [[CrossRef](#)] [[PubMed](#)]

30. Van, D.; Asta, M.; Ceder, G. The Alloy Theoretic Automated Toolkit: A User Guide. *Calphad* **2002**, *26*, 539–553.
31. Jiang, S.; Wang, H.; Wu, Y.; Liu, X.; Chen, H.; Yao, M.; Gault, B.; Ponge, D.; Raabe, D.; Hirata, A.; et al. Ultrastrong Steel via Minimal Lattice Misfit and High-Density Nanoprecipitation. *Nature* **2017**, *544*, 460–464. [[CrossRef](#)]
32. Sumitomo, T.; Cáceres, C.H.; Veidt, M. The Elastic Modulus of Cast Mg–Al–Zn Alloys. *J. Light Met.* **2002**, *2*, 49–56. [[CrossRef](#)]
33. Matsumuro, A.; Murata, K.; Sakai, K.; Senoo, M. Elastic and Superconducting Properties of Supersaturated Al–Si and Al–Ge Solid-Solution Alloys Treated under a 5.4 GPa Pressure. *J. Mater. Sci.* **1993**, *28*, 5836–5842. [[CrossRef](#)]
34. Ravi, C.; Wolverton, C.; Ozoliņš, V. Predicting Metastable Phase Boundaries in Al–Cu Alloys from First-Principles Calculations of Free Energies: The Role of Atomic Vibrations. *Europhys. Lett.* **2006**, *73*, 719–725. [[CrossRef](#)]
35. Amir Khanlou, S.; Ji, S. A Review on High Stiffness Aluminum-Based Composites and Bimetallics. *Crit. Rev. Solid State Mater. Sci.* **2020**, *45*, 1–21. [[CrossRef](#)]
36. Tsubakino, H.; Nozato, R.; Sakurai, T.; Hasegawa, Y.; Hayashi, Y. Precipitation of metastable δ' in Al–1.9Li–2.5Mg alloy. *Mater. Sci. Technol.* **1994**, *10*, 222–226. [[CrossRef](#)]
37. Huang, X.; Guan, B.; Wang, B.; Zang, Y. Hot tensile deformation behavior, fracture mechanism and microstructural evolution of 2195 Al–Li alloy. *J. Alloys Compd.* **2023**, *946*, 169426. [[CrossRef](#)]
38. Guo, X.; Wen, S.H.; Jiao, H.; Wu, S. Effect of aging treatment on microstructure and mechanical properties of TIG welded joints of 2195–T8 Al–Li alloy. *Mater. Charact.* **2023**, *196*, 112576. [[CrossRef](#)]
39. Xu, X.; Wu, G.; Zhang, L.; Tong, X.; Zhang, X.; Sun, J.; Li, L.; Xiong, X. Effects of heat treatment and pre-stretching on the mechanical properties and microstructure evolution of extruded 2050 Al–Cu–Li alloy. *Mater. Sci. Eng. A* **2022**, *845*, 143236. [[CrossRef](#)]
40. Noble, B.; Bray, S.E. On the $\alpha(\text{Al})/\delta'(\text{Al}_3\text{Li})$ Metastable Solvus in Aluminium–Lithium Alloys. *Acta Mater.* **1998**, *46*, 6163–6171. [[CrossRef](#)]
41. Tang, J.; Yi, Y.; He, H.; Huang, S.; Wang, H.; Zhang, J. Effect of forging pretreatment on the microstructures and mechanical properties of the Al–Cu–Li alloy. *J. Alloys Compd.* **2023**, *965*, 171379. [[CrossRef](#)]

Disclaimer/Publisher’s Note: The statements, opinions and data contained in all publications are solely those of the individual author(s) and contributor(s) and not of MDPI and/or the editor(s). MDPI and/or the editor(s) disclaim responsibility for any injury to people or property resulting from any ideas, methods, instructions or products referred to in the content.